Applied Surface Science 499 (2020) 143908

Contents lists available at ScienceDirect

Applied Surface Science

journal homepage: www.elsevier.com/locate/apsusc

Full length article

The influence of protein concentration, temperature and cathodic polarization on the surface status of CoCrMo biomedical grade alloys

Righdan Namus[a,b,*], John Nutter[a], Jiahui Qi[a], W. Mark Rainforth[a]

[a] Department of Materials Science and Engineering, The University of Sheffield, Mappin Street, Sheffield S1 3JD, UK
[b] Faculty of Engineering, Wasit University, Kut, Iraq

ARTICLE INFO

Keywords:
CoCrMo implants
Protein adsorption
Oxide layer resistivity
Adhesion force

ABSTRACT

CoCrMo alloys have been widely used in hip replacements. On the one hand they have exhibited excellent long-term survival rates, but recently high failure rates have been observed, associated with adverse local tissue reactions. It is still a puzzle why CoCrMo alloys sometimes work very well, while at the other times the failure rate is unacceptably high. The current work aims to investigate the influence of protein adsorption on the oxide layer properties and consequently on corrosion behaviour of CoCrMo biomedical grade alloys in different surface and media conditions. Electrochemical Impedance Spectroscopy (EIS), SEM and AFM were employed to characterise the surfaces. TEM was also used to reveal the subsurface chemical composition. The results showed a significant drop in the resistance of the oxide layer on the surfaces after some cathodic potential polarization. It was also shown that higher protein content and temperature reduced the oxide layer/metal surface interface resistivity. EDX quantitative chemical composition spot analysis of the subsurface after cathodic polarization showed a depletion of chromium in the outermost layer. AFM imaging and peak-force quantitative nano-mechanical mapping QNM revealed lower adhesion forces for a relatively thick proteinaceous adsorbed layer on the surface after high cathodic polarization in particular at 50 °C.

1. Introduction

CoCrMo alloys have been widely used in total hip replacements (THRs) and hip resurfacing treatments for many years. There have been many cases where the joints have performed very well and have lasted for > 20 years [1–3]. However, higher than the expected failure rates of metal-on-metal (MoM) hip replacements have been observed, with failures associated with metal debris and ion release from these alloys [4,5]. In 2010 the Medicines and Healthcare Products Regulatory Agency (UK) and in 2011 the Food and Drug Administration (US) issued alerts for all MoM hip replacements, respectively, with concerns about the adverse local tissue reactions (ALTR) to metal ions, resulting in a sharp drop in the use of the MoM market. This has now become a subject of intense interest with much debate about why the survivability of MoM changed so abruptly, with much focus on the joint design as well as the material performance.

Protein concentration in synovial fluid is reported to increase significantly with infections, particularly for those people with rheumatoid arthritis [6,7]. Equally, the local temperature in hip joints is reported to rise as high as 50 °C [8]. These two effects might weaken the protective oxide layer and thereby make it prone to local break down. This is in addition to the damage caused by entrapped species that can lead to scratching of the surface. The most extreme events will occur while walking or running. Where damage of the protective surface oxide layer occurs, the entire system will be cathodically polarised due to the much lower potential for the bare metal areas. The severity of this event depends, among other things, on the number and the position of these broken oxide layer areas (scratched surfaces). Thus, it is expected that the surface could work at a range of cathodic potentials for some time.

The existence of salts and protein in the electrolyte has a major effect on corrosion properties of passive metals and alloys. The corrosion rate of austenitic stainless steel was reported to be increased significantly when protein exists in the solution. The polarization resistance decreases with protein concentration followed by plateau after a threshold (Langmair adsorption isotherm) in the temperature range 299–343 K. The mechanism of adsorption has been proposed as the interaction of negatively charged carboxylate group of the protein with austenitic stainless steel surface involving charge transfer and thus strong adsorption (chemisorption) [9,10].

The adsorption process is such a complex phenomenon as it is influenced by many factors including chemical and physical properties of the sorbent surface (hydrophobicity [11], surface polarity [12],

* Corresponding author at: Department of Materials Science and Engineering, The University of Sheffield, Mappin Street, Sheffield S1 3JD, UK.
E-mail address: raghdan@uowasit.edu.iq (R. Namus).

https://doi.org/10.1016/j.apsusc.2019.143908
Received 11 July 2019; Received in revised form 12 August 2019; Accepted 7 September 2019
Available online 12 September 2019
0169-4332/

chemical composition of the oxide layer [13] etc.), the structural stability of protein [11,14], and the potential [15]. The adsorption of fibrinogen and bovine serum albumin BSA on commercial pure (CP) titanium over the temperature range 295–343 K and protein bulk solution concentration (0–0.4 g/L) has been studied [16]. A direct relation between surface charge density and protein surface concentration has been shown, indicating that the process is chemisorption. The two proteins showed different adsorption behaviour. BSA exhibits a bimodal isotherm, whilst fibrinogen showed a single saturation plateau which had a 2× greater affinity for adsorption. The process of protein adsorption appears to be endothermic and entropically controlled.

Vidal et al. [17] successfully used Electrochemical Impedance Spectroscopy (EIS) to investigate the effect of BSA adsorption on CoCrMo alloys. Charge transfer resistance was found to be very sensitive to the amount of protein adsorption. The corrosion activation energy was reported to decrease with protein adsorption until a particular point (500 mg/L) at which it significantly increased. The inhibition behaviour of protein at relatively high solution bulk protein concentration was rationalized on the basis that the protein covered the surface, which blocks mass transport of corrosion products and/or oxygen. The entropically controlled nature was also reported to be dominated as the thermodynamic driving force for the adsorption of protein on CoCrMo alloys, as has been observed on austenitic stainless steel [10] and titanium [16]. The obvious gain in entropy clearly indicates conformational changes of adsorbed protein which could arise from protein structural unfolding on the adsorbate.

The adsorption of bovine serum albumin on a CoCrMo alloy is reported to be sensitive to the surface passivation. Increasing immersion time at the OCP and applying a passive potential both led to a reduction in the amount of adsorbed protein. The deliberately passivated surfaces adsorbed less BSA compared to those surfaces that have not developed a stable oxide layer [18]. Igual and Mischler [19] suggested a competitive adsorption mechanism of phosphate buffered saline PBS ions and albumin on the surface of CoCrMo alloy. They tested the adsorption at OCP and passive potential in different solutions (NaCl, and PBS, with and without albumin). At passive potential, the oxide layer chemical composition and thickness were not affected by the solution chemistry. However, the adsorbed layer resistance and capacitance showed a significant dependence on solution composition. The extreme case was at PBS solution that gave the highest adsorbed layer resistance. This resistance was even higher than the oxide layer resistance making the adsorbed layer is the rate limiting factor in the corrosion process. This has been attributed to the very compact layer of the adsorbed phosphate ions layer that covered the surface and probably efficiently blocked mass transport. However, this compacted layer cannot be achieved with giant molecules like albumin. The presence of albumin has the same effect, but to a lesser extent, in which case the oxide layer remains the most important factor in blocking mass transport. Conversely, at OCP the nature of the passive film was affected by the chemical composition of the solution. The formation condition of the oxide layer is thought to be the reason for this. The fast growth of the oxide layer at passive potential could limit the interaction of phosphate ions and albumin, which is not the case at OCP where this growth is relatively slow.

Surprisingly, the effect of the value of the cathodic potential and the protein concentration in the synovial fluid on the oxide layer properties has not been investigated. Thus, the current work was carefully designed to study the effect of cathodic polarization of CoCrMo biomedical grade alloy in simulated body fluid on the adsorption of protein on the surface, and its consequence on the protective oxide layer status. This was explored over a range of protein concentrations and temperatures that are realistic to the human body.

Table 1
chemical composition of the CoCrMo alloy used in the work.

Element	Co	Cr	Mo	Mn	C	Fe	Si	Ni
wt%	64.91	27.48	5.25	0.45	> 0.05	0.32	0.42	0.16

2. Experimental work

2.1. Material

The chemical composition of as-cast low carbon CoCrMo alloy, supplied in 15 mm diameter bar form, is shown in Table 1. Samples were sectioned into 3 mm thick discs. All samples were mechanically ground in the standard manner, finishing with 1 µm diamond and SilcoTM to ensure the best possible surface finish with the minimum residual surface damage. Optical profilometry (ContourGT 3D Optical Microscope, Bruker, US) was used to measure the surface roughness of the samples after polishing, which was always < 10 nm R_a for all starting surfaces.

2.2. Work procedure

Fig. 1 shows the map of the current work. To simulate body fluids, new born calf bovine serum (First Link (UK) Ltd.) was diluted and buffered to 25, 40 and 50 vol% in an aqueous solution of phosphate buffer saline PBS (Sigma-Aldrich) giving ≈15, 25, and 30 g/L protein concentrations respectively. Ultrapure water (Alfa Aesar) was used in the preparation of the solution. The solution pH was 7.4. The protein concentrations were chosen to cover the real protein content in synovial fluid for a healthy human and a human at different disease conditions [6,7]. 15 g/L protein concentration at 37 °C considered as the control experiment to be compared with other testing conditions because it represents the working conditions for healthy human at normal case. All the tests were done at 37 °C and 50 °C.

Open circuit potential (OCP) and two cathodic potentials namely −0.7 V, and −0.9 V were tested. The potentials were chosen after many trial and error experiments in 100 mV step cathodic polarization starting from OCP to get different electrochemical impedance spectral response. Note that the highest used cathodic potential in the current work was only about 400 mV more cathodic that OCP (OCP vary between −0.5 V to −0.6 V vs. SCE for all testing solutions).

Fig. 2 shows the work sequence for each experiment. The polished sample is immersed in a preheated solution at the test temperature and protein concentration for 1 h waiting for OCP to be stabilized. EIS is taken for the surface at OCP. The surface was then step polarised to the test cathodic potential for 30 min and the EIS was taken at this potential. Half an hour cathodic polarization was chosen because it equates to the normal walking time. This was followed by removing the cathodic potential and waiting for 2 h to obtain a stable OCP. Finally, EIS was taken at this point. The data showed good reproducibility with $n = 2$. The standard error of the mean was calculated for each data point.

2.3. Electrochemical investigation

Electrochemical characterization of the surfaces was carried out by using standard three electrode traditional corrosion cell with SCE as a reference electrode (its potential vs. SHE is 0.242 V), two graphitic rods as the counter electrode, and the material being tested as working electrode. The volume of the cell was 600 mL. EIS was undertaken using a VersaSTAT 3F Potentiostat Galvanostat (Princeton Applied Research, US). The frequency range was 100 kHz to 15 mHz in perturbation amplitude 10 mV at 10 points per frequency decade. ZView software was used to model the data with appropriate electric equivalent circuit EEC.

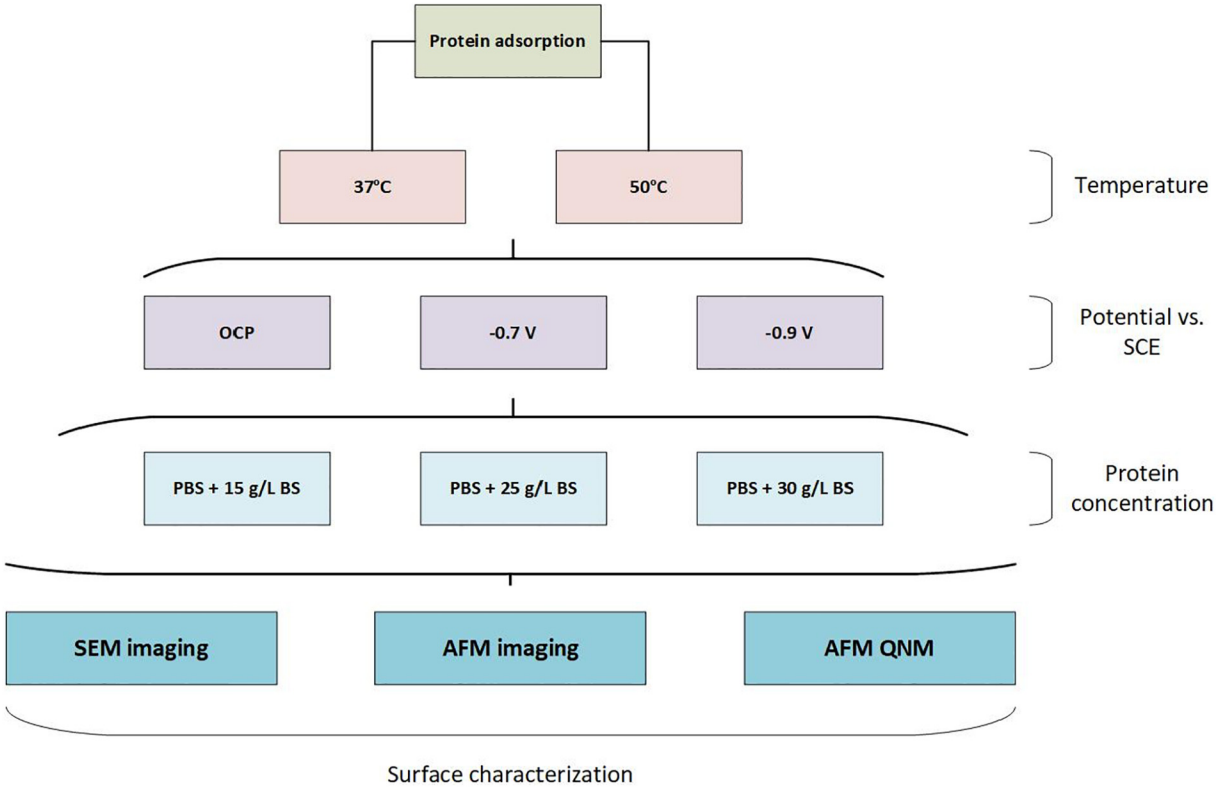

Fig. 1. The work map showing the temperatures, the potentials and the protein concentration used in the current work.

2.4. Surface characterization

The surfaces were imaged via SEM (FEI, Inspect F50, the Netherlands). The morphology of the surfaces was revealed by using multimode AFM (Bruker, US) peak force tapping mode. 0.5 N/m cantilever spring constant tip (Scanasyst-Air Bruker) was used for imaging the surfaces. Peak force quantitative nanomechanical mapping QNM was employed to provide deformation and adhesion maps for the surfaces coved by different thickness of the proteinaceous adsorbed layer. The tip cantilever spring constant used in QNM was 200 N/m (Rtespa-525).

2.5. FIB/TEM subsurface chemical composition investigation

TEM samples were removed from the surface after −0.9 V cathodic polarization at 30 g/L protein content solution and 50 °C by focused ion beam (FIB) (FEI Quanta 200 3D SEM/FIB the Netherlands). Carbon deposition was applied on the region of interest to prevent Ga^+ implantation and sputter erosion of the top portion of the surface. Various Ga^+ ion beams (7–2.5 nA) were used for rough milling with a 30 pA Ga^+ ion beam finishing.

TEM observation was obtained using a JEOL JEM-F200 (JEOL, Tokyo, Japan) operated in STEM mode at 200 kV. Spot quantitative analysis was also performed at a closest possible point to the deposited proteinaceous layer and at other points in the bulk.

3. Results

3.1. Surfaces electrochemical characterization

Fig. 3 shows an EIS spectrum for surfaces at starting OCP (the surfaces before any cathodic polarization and after stabilisation of the potential) and at OCP after cathodic polarization to −0.7 V and −0.9 V at 37 °C (EIS was taken after 2 h of removing the cathodic potential). For all tests, Nyquist plots show a semicircle with the centre depressed below the x-axis clearly revealing the non-perfect capacitive behaviour of the surface layer. The semicircles intersect the x-axis at high frequencies giving the solution resistance R_s. At very low frequencies (which cannot be reached experimentally but can be extracted by using electric equivalent circuit modelling), the semicircle should intersect

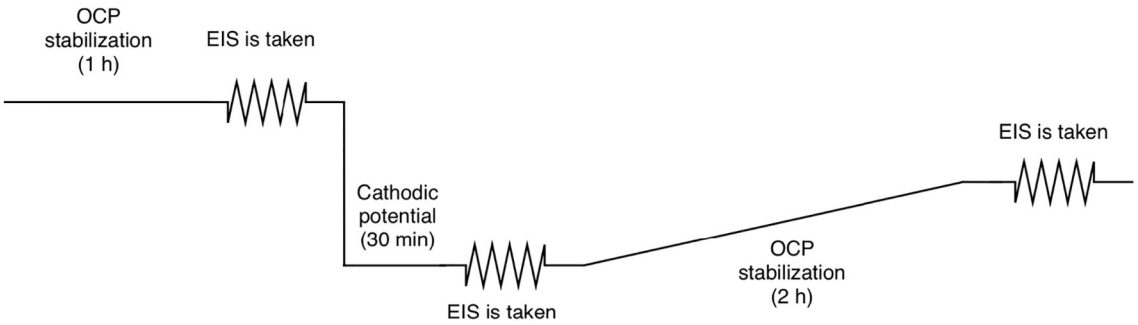

Fig. 2. Work procedure for each experiment.

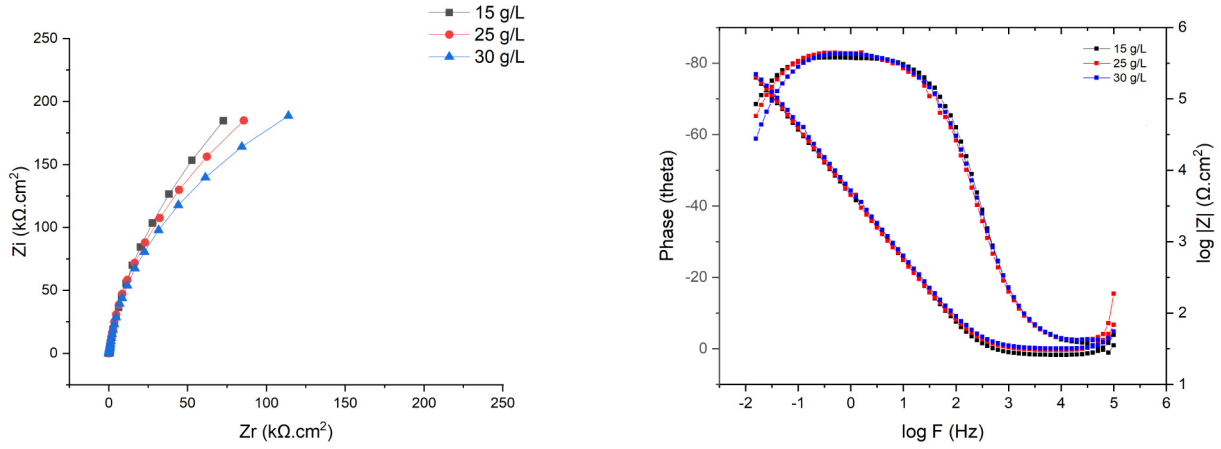

Starting OCP

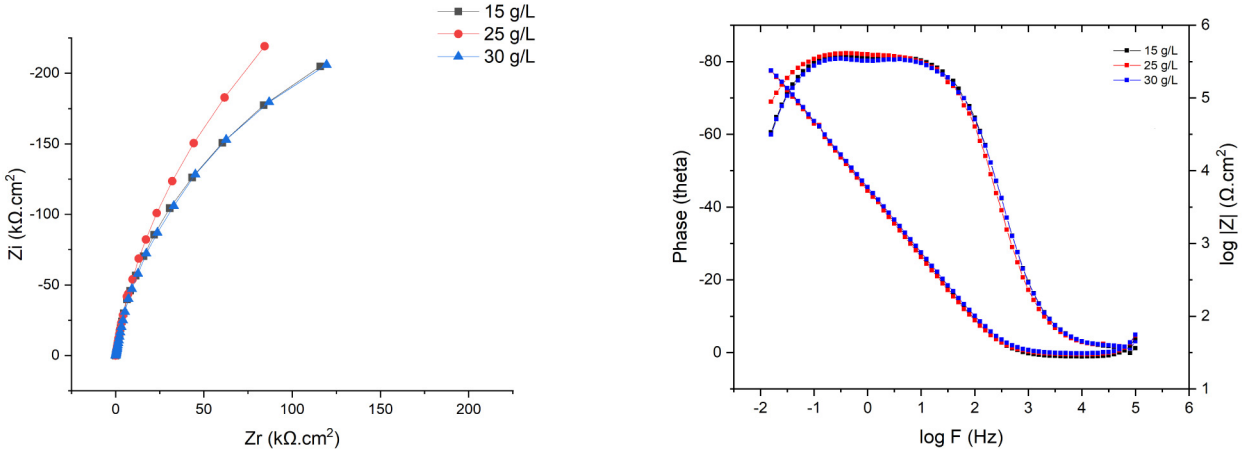

OCP after -0.7V

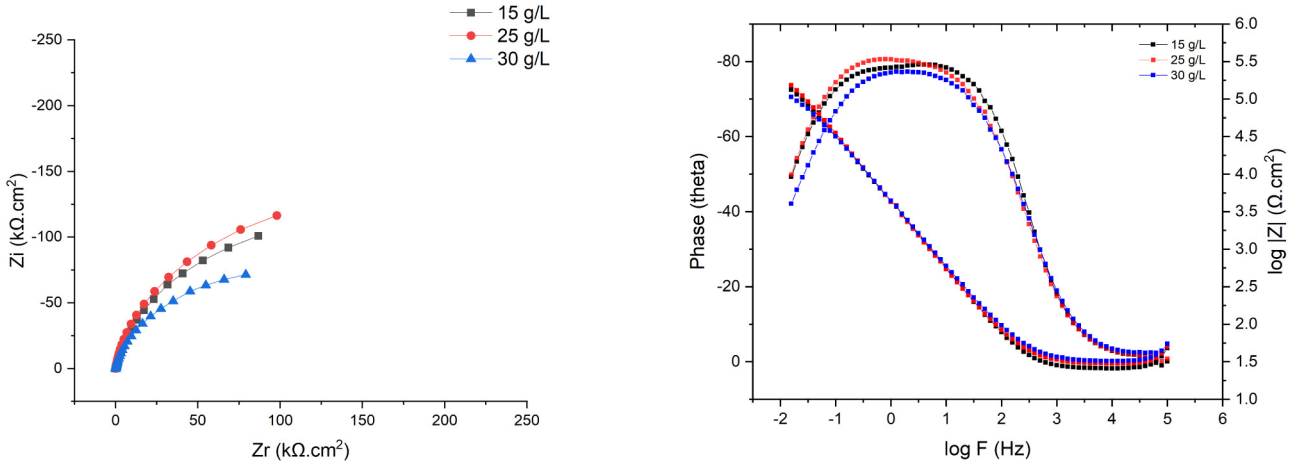

OCP after -0.9V

Fig. 3. Nyquist plot (on the left), and Bode plot (on the right) for CoCrMo alloy in simulated body fluid tested at starting OCP, OCP after −0.7 V cathodic polarization (after 2 h of stopping the polarization) and after −0.9 V cathodic polarization (after 2 h of stopping the polarization) at 37 °C.

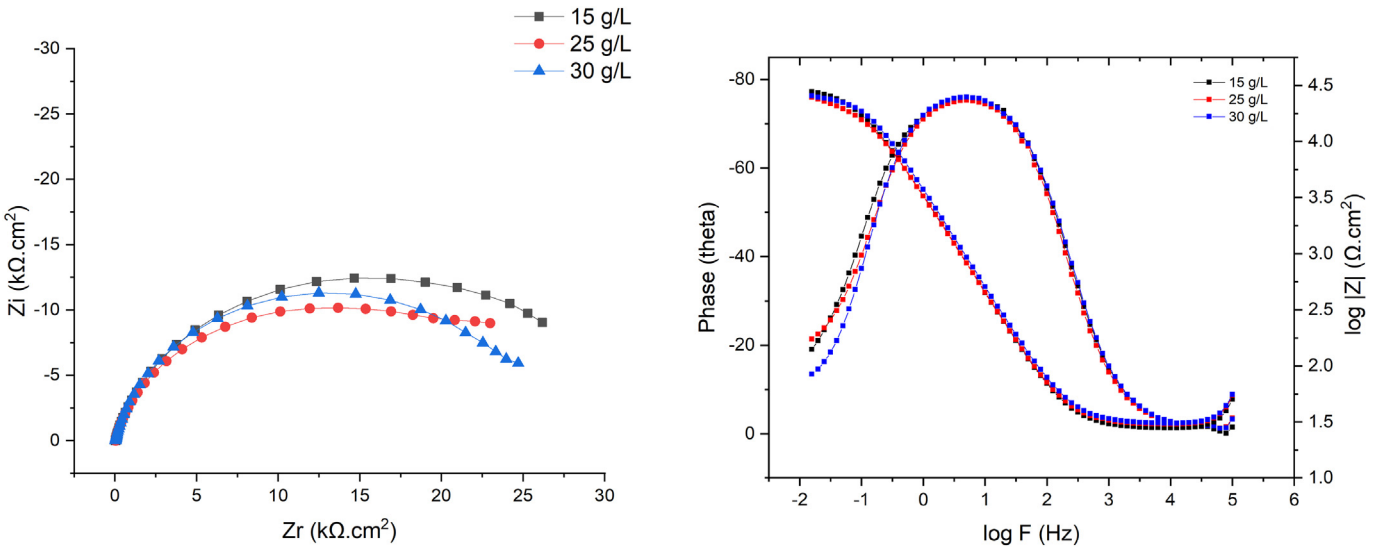

Fig. 4. Nyquist plot (on the right) and Bode plot (on the left) for cathodically polarised surfaces at −0.7 V taken after half an hour of polarization at 37 °C.

the x-axis again to give the solution resistance plus the total surface resistance ($R_s + R_t$). At intermediate frequencies, the imaginary part starts to increase, indicating the capacitive behaviour of the surface. A Bode plot shows that the material exhibits a plateau at high and low frequencies giving R_s and ($R_s + R_t$) respectively. At intermediate frequencies, the curve is a straight line with a slope close to −1 in all cases. The phase shift gives the same indication as it is close to zero at both high and low frequencies, while it peaks at intermediate frequencies as the imaginary component of the impedance increases.

Fig. 4 is an EIS spectrum for the surfaces at −0.7 V cathodic polarization. The size of the semicircle in the Nyquist plot notably decreased at this potential compared to that at the starting OCP condition, denoting the effect of this potential on the properties of the oxide layer.

Further cathodic polarization to −0.9 V, Fig. 5, showed a significant effect on the oxide layer with the appearance of diffusion elements at low frequencies. The angle of the tail in the Nyquist plot is < 45° which might be interpreted that diffusion occurs in the surface deposited layer.

The equivalent electric circuit EEC for modelling the EIS data at starting OCP and OCP after −0.7 V and −0.9 V cathodic polarizations is shown in Fig. 6. The circuit is the solution resistance R_s in series with a parallel combination of constant phase element CPE_{ad}, and the

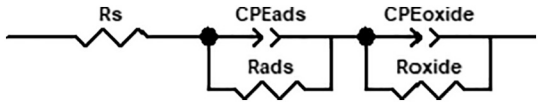

Fig. 6. EEC used in simulating the EIS data.

resistance R_{ad} of the surface adsorbed layer which is in turn in series with another same combination for the oxide layer (R_{oxide} and CPE_{oxide}). The EIS spectrum at the cathodic polarization was not modelled to EEC, but shown for the sake of comparison. All the results of EIS data modelling are tabulated in Table 2 and Table 3.

Fig. 7 shows the resistance of the oxide layer R_{oxide} at starting OCP, and OCP after cathodic polarization at 37 °C and 50 °C, calculated from fitting EIS spectrum to the EEC. R_{oxide} for starting OCP decreased with increasing the protein concentration and temperature. At 37 °C, the surfaces at OCP after −0.7 V polarization did not exhibit that much difference in R_{oxide} compared to starting OCP at all tested protein content. Nevertheless, R_{oxide} was enhanced after −0.7 V cathodic polarization at 50 °C particularly at 25, 30 g/L protein concentration in comparison to ones at starting OCP at the same temperature. R_{oxide} was enhanced by about 1.5, and 3 times after −0.7 V polarization at 25 g/L,

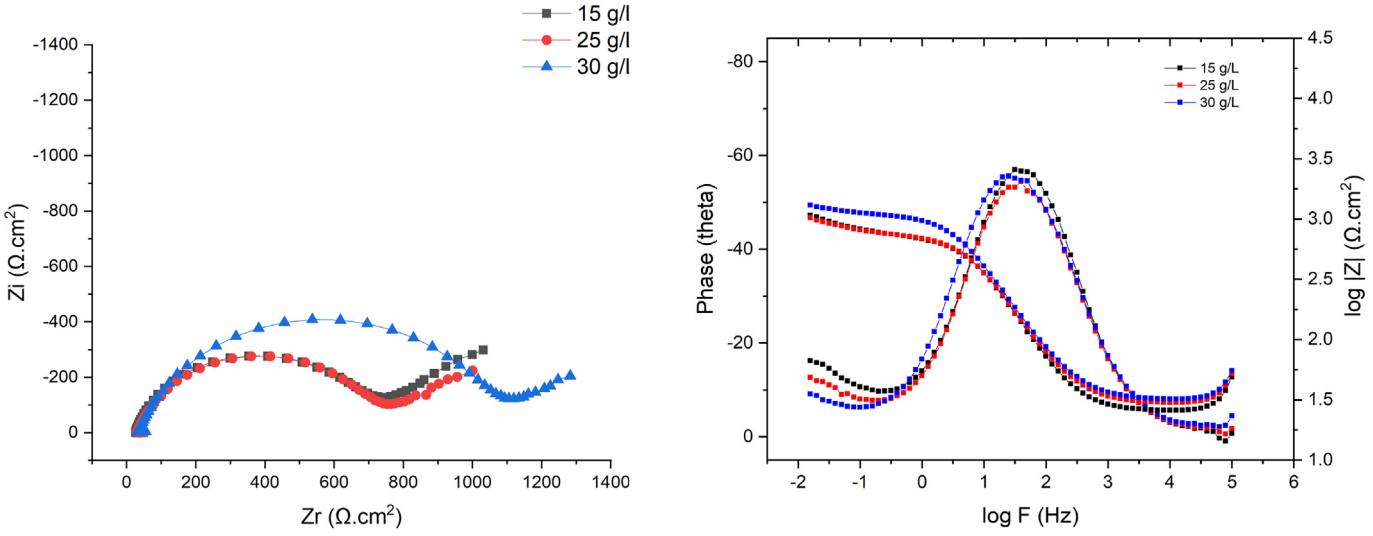

Fig. 5. Nyquist plot (on the right) and Bode plot (on the left) for cathodically polarised surfaces at −0.9 V taken after half an hour of polarization at 37 °C.

Table 2
EIS model parameters for CoCrMo alloy in different protein content solutions and at OCP, OCP after −0.7 V cathodic polarization and OCP after −0.9 V cathodic polarization at 37 °C.

Protein content (g/L)	Chi-Sqr × 10^{-4}	Sum-Sqr × 10^{-2}	R_s (Ω)	Q_{ads} (μF·cm^{-1}·$s^{\alpha-1}$)	α_{ads}	R_{ads} (Ω·cm^2)	Q_{oxide} (μF·cm^{-1}·$s^{\alpha-1}$)	α_{oxide}	R_{oxide} (kΩ·cm^2)
Starting OCP									
15	4.5	4.8	25	134	0.82	55 ± 5	42	0.92	783 ± 27
25	26	27	30	438	0.83	15 ± 1	39	0.93	633 ± 8.5
30	8	8.6	31	458	0.80	21 ± 2.5	33	0.93	507 ± 17
OCP After −0.7 V									
15	4.3	4.7	27	540	0.77	483 ± 52	32	0.94	580 ± 28
25	30	33	29	258	0.87	430 ± 39	34	0.95	762 ± 30
30	1.9	2.2	30	302	0.80	1023 ± 95	32	0.94	568 ± 17
OCP after −0.9 V									
15	3.1	3.5	25	453	0.84	1035 ± 82	47	0.91	235 ± 9
25	8.3	9.5	29	188	0.77	24,330 ± 2180	54	0.91	224 ± 10
30	5.5	6.2	32	94	0.81	56,000 ± 5537	85	0.93	175 ± 8

and 30 g/L protein concentration respectively.

In contrast, the polarization to −0.9 V cathodic potential had a significant negative impact on R_{oxide} at both tested temperatures. R_{oxide} decreased to one third (or even more in some cases) in comparison to its value at starting OCP. The resistance of the adsorbed protein layer R_{ads} did not contribute to the total resistance of the surface (Fig. 8). Its value can be neglected at starting OCP and OCP after −0.7 V cathodic polarization. However, its contribution increased at OCP after −0.9 V cathodic polarization with protein content at the two tested temperatures. At OCP after −0.9 V and 50 °C, R_{ads} was half of R_{oxide} indicating that there was a compacted adsorbed proteinaceous (or possibly a mixture of protein and salt) layer covers the surface.

3.2. Calculating the film thickness and the resistivity of the oxide film by using the graphical method

The electric equivalent circuit EEC is commonly used to analyse EIS data. Many systems show a behaviour attributed to surface heterogeneity. Thus, CPE is usually used to fit EIS data. Different expressions were proposed in the literature to obtain the capacitance from CPE value with a debate about the accuracy [20,21]. Thus, the graphical method is used in the current work to get a better understanding of the system being investigated. The capacitance of the oxide layer can be accurately extracted from the complex capacitance plane after the correction by removing the solution resistance R_s as following [22–26]:

$$C(\omega) = \frac{1}{j\omega(Z(\omega) - R_s)}$$

$$C_{re} = -\frac{Z_{im}}{\omega((Z_{re} - R_s)^2 + Z_{im}^2)}$$

$$C_{im} = -\frac{Z_{re}}{\omega((Z_{re} - R_s)^2 + Z_{im}^2)}$$

R_s is extracted from the Nyquist plot by extrapolation the curve to intersect the real axis. In the corrected complex capacitance plane, the capacitance value of the oxide layer is the intersect point on the real axis at high frequency (Fig. 9 shows an example). Once the accurate capacitance of the oxide layer is known, the thickness can be calculated by the following formula [23]:d denotes the film thickness, A is the active area, ε_0 vacuum permittivity (8.85×10^{-14} F/cm), and ε is the film dielectric constant taken as 12.5 for chromium oxide [27]. The protective oxide film on CoCrMo alloys is reported to be mostly chromium oxide [28].

The resistivity of the oxide film/metal surface interface, ρ_0, is calculated from the characteristic frequency f_0, which is the frequency at the maximum imaginary part of the impedance or the frequency at 45° phase shift. Further details of this calculation can be found elsewhere [23,29].

$$\rho_0 = \frac{1}{2\pi\varepsilon\varepsilon_0 f_0}$$

Table 3
EIS model parameters for CoCrMo alloy in different protein content solutions and at OCP, OCP after −0.7 V cathodic polarization and OCP after −0.9 V cathodic polarization at 50 °C.

Protein content (g/L)	Chi-Sqr × 10^{-4}	Sum-Sqr × 10^{-2}	R_s (Ω)	Q_{ads} (μF·cm^{-1}·$s^{\alpha-1}$)	α_{ads}	R_{ads} (Ω·cm^2)	Q_{oxide} (μF·cm^{-1}·$s^{\alpha-1}$)	α_{oxide}	R_{oxide} (kΩ·cm^2)
Starting OCP									
15	5.8	6.3	24	578	0.75	65 ± 6	29	0.93	669 ± 26
25	6	6.6	23	670	0.72	70 ± 8	33	0.91	489 ± 44
30	3.7	4.1	29	547	0.77	30 ± 3	40	0.93	311 ± 34
OCP after −0.7 V									
15	2.7	2.9	19	259	0.85	17 ± 1.3	39	0.93	727 ± 59
25	11	13	29	121	0.78	62 ± 5.7	29	0.93	820 ± 42
30	6.4	7.2	29	220	0.75	64 ± 4.9	33	0.93	929 ± 65
OCP after −0.9 V									
15	1.5	1.6	25	287	1.01	1841 ± 147	47	0.87	160 ± 10
25	3.4	3.8	23	288	0.73	3793 ± 341	41	0.86	151 ± 6
30	14	16	22	186	0.70	48,662 ± 5100	64	0.92	88 ± 6

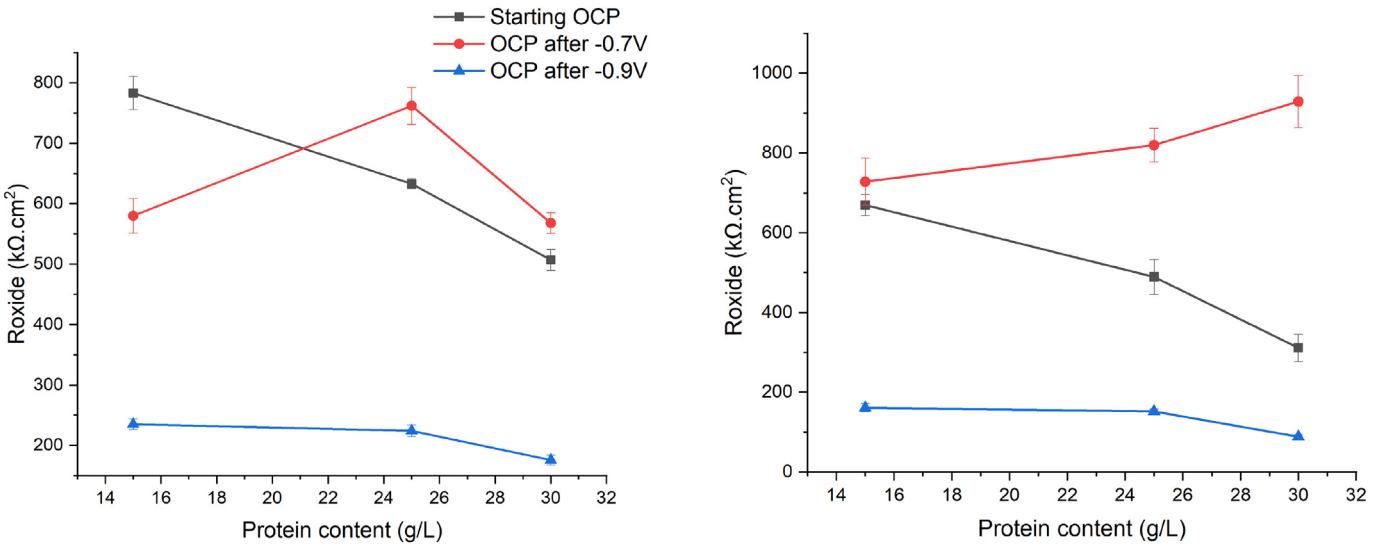

Fig. 7. R_{oxide} for CoCrMo in different protein content solutions at starting OCP and OCP after cathodic polarization for different protein content at 37 °C (on the left side) and 50 °C (on the right side).

The lowest frequency used in this work was 15 mHz. Going to a lower frequency takes too long time, which could affect the surface condition. For laboratory conditions, the protein is degraded during long term testing. This might affect the adsorption phenomenon (the subject of the study) on the surface. At the lowest frequency used in this work, the experimental data does not reach the peak of the imaginary part of the impedance at OCP. Thus, the best fitting curve for the data was used to get f_0 which was extracted from the fitting curve at 45° phase shift. An example of this is shown in Fig. 10. All the results of the graphical method are tabulated in Tables 4 and 5.

Fig. 11 shows the oxide film thickness and film/metal interface resistivity at 37 °C and 50 °C for the surfaces at starting OCP and OCP after −0.9 V calculated from the graphical analysis method. The calculation was done for only one set of tests because the data already showed good reproducibility (Fig. 7). The oxide film thickness showed no change at starting OCP and OCP after −0.9 V cathodic polarization at 37 °C. However, it became thicker at 50 °C with increasing protein content for both starting OCP and OCP after −0.9 V.

The resistivity of the oxide film/metal interface, on the other hand, is within the resistivity range for insulators for all tests. However, the resistivity of starting OCP exhibited a noticeable decrease with increasing protein content and temperature to the point that it was more than one order of magnitude less at the highest tested protein concentration and temperature compared to that at starting OCP at 15 g/L protein content and 37 °C test (control test).

The oxide film/metal surface interface was always negatively affected by cathodic polarization to −0.9 V for all tested protein content and temperature, as shown in Fig. 11. Moreover, the oxide film/metal surface interface resistivity for OCP after −0.9 V, more or less, is protein concentration and temperature independent. The results of the graphical method are in good agreement with EEC results since both methods gave the same trend.

3.3. SEM and AFM characterization

The surfaces after −0.9 V polarization were imaged using SEM, Fig. 12. The surfaces appeared to be almost entirely covered by the adsorbed layer. AFM Peak Force tapping mode was employed to reveal the morphology of the surface and the adsorbed layer, Fig. 13. AFM imaging was undertaken for the surfaces after the two cathodic

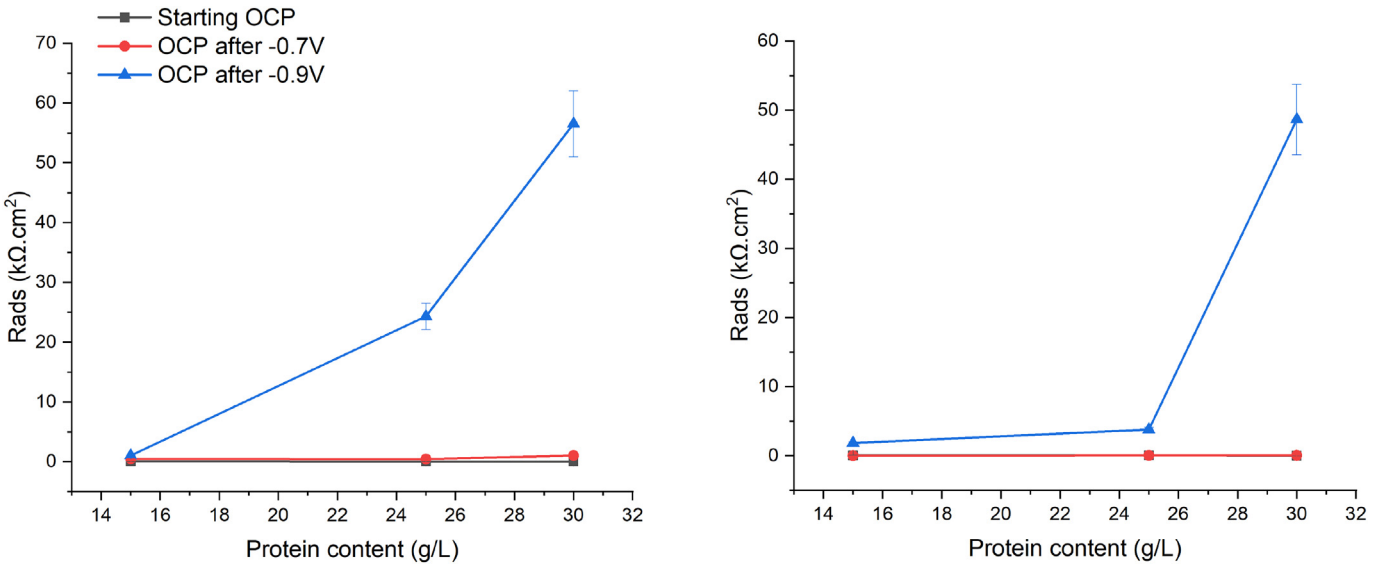

Fig. 8. R_{ads} at 37 °C (on the left hand) and 50 °C (on the right hand) for starting OCP and OCP after cathodic polarization at different protein concentration solutions.

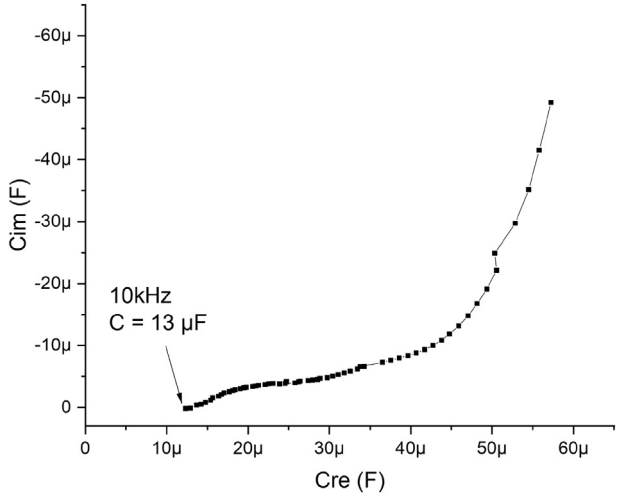

Fig. 9. Complex capacitance plane for the surface at 15 g/L protein concentration solution at OCP after −0.9 V test (as an example of calculating the capacitance of the oxide layer. The sample surface area is 1 cm^2.

$$C = \varepsilon . \varepsilon_0 . \frac{A}{d}$$

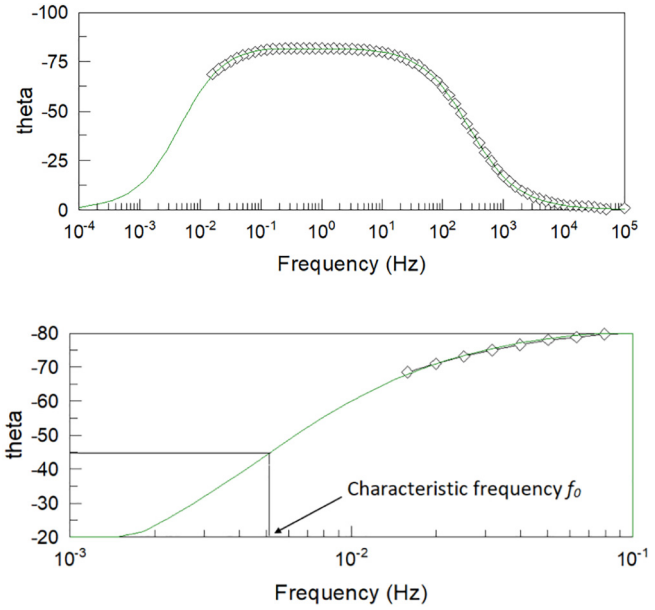

Fig. 10. An example for extraction method of f_0 from the fitting curve of EIS spectrum.

Table 4
EIS graphical analysis method results at 37 °C.

Protein content (g/L)	C ($\mu F/cm^2$)	d (nm)	f_0 (mHz)	ρ_0 (Ohm.cm)	α
Starting OCP					
15	15	0.7	2	4.5×10^{14}	0.9
25	14	0.8	6	1.51×10^{14}	0.91
30	13	0.85	9	1×10^{14}	0.9
OCP after −0.9 V					
15	13	0.85	11	7.8×10^{13}	0.89
25	13	0.8	15	6×10^{13}	0.87
30	12	0.9	20	4.5×10^{13}	0.83

polarizations (−0.7 V and −0.9 V). The starting OCP surfaces were not imaged because there was no difference between these surfaces and those after −0.7 V cathodic polarization. The extreme cases were chosen for imaging to show the differences in the morphology of the adsorbed layer. The figure reveals that all the surfaces were covered by an adsorbed layer after testing at the two cathodic potentials. Moreover, the adsorbed layer appeared to be more compacted after −0.9 V cathodic polarization for the two tested temperatures.

Deformation and adhesion maps for the surfaces after −0.7 V 15 g/L at 50 °C, after −0.9 V 15 g/L at 37 °C and after −0.9 V 30 g/L at 50 °C are shown in Fig. 14. The maps were taken using the same tip and the same calibration to make them directly comparable. The maps for the surfaces at 37 °C after −0.9 V 15 g/L sample clearly show that the thicker adsorbed layer (the higher regions in the height map) exhibited higher deformation and lower adhesion. At 50 °C the deformation map for the surface after −0.9 V 30 g/L shows that the deformation range was about 4 nm, whereas it was about 0.7 nm (less than one fourth) at the surface after −0.9 V 15 g/L and 37 °C. Additionally, the adhesion force maps clearly suggested that the lowest adhesion force was at the surface after −0.9 V at 30 g/L and 50 °C. All these indicate that the thickest and most compacted layer was adsorbed on the surface after −0.9 V and 30 g/L protein content at 50 °C. To this end, it can be concluded that a thicker adsorbed layer is less adhesive, which will have implications for friction and wear of these surfaces.

3.4. Chemical composition of the subsurface

Fig. 15 is a TEM image for the outermost subsurface of the surface after −0.9 V cathodic polarization at 30 g/L protein content solution and 50 °C. The figure clearly shows a proteinaceous layer deposited on the surface with about 5 nm thickness. Quantitative chemical analysis for many points was undertaken just below the deposited layer and other points on the substrate, as shown in Fig. 16 and Table 6. The chromium mass fraction reduced by about 3% in the region just next to the proteinaceous layer which might be the reason of the decrease in the resistivity of the oxide layer after cathodic polarization to −0.9 V. The passive behaviour of CoCrMo alloys was shown to be due to the formation of an oxide film that mainly consists of Cr_2O_3. Furthermore, cobalt was the main element to be dissolved, apart from in the transpassive region where all elements in the alloy were dissolved. Therefore, the passive behaviour of these alloys is strongly influenced by chromium, and the dissolution behaviour is mainly affected by cobalt [28]. Cobalt was present mainly as CoO and molybdenum as MoO_3. Molybdenum is added to these alloys as a strengthening agent [30], but does nothing to improve the corrosion behaviour.

4. Discussion

Interestingly, the key variables examined in the current work, namely the protein concentration, the temperature and the cathodic potential, have not been investigated in the literature, despite being the key working variables of metallic implants. Many researchers have studied the adsorption of protein over a range of temperature and its effect on corrosion properties of biometallic implants in materials such as stainless steel [9,10], CP titanium [16] and CoCrMo alloys [18,19]. However, they focused on the adsorption phenomena using low protein content solutions. The current work attempted to simulate the real service condition by proposing the real concentration of protein in the human body and its variation.

The current work clearly showed that the resistance of the surface oxide film of CoCrMo biomedical grade alloy to relatively high cathodic potential in PBS + BS solution considerably decreased. The cathodic polarization of metallic hip or knee artificial replacements can occur for some time, as explained in the introduction of this paper. The two different analysis methods used in this work revealed the same trend in surface behaviour. The EEC analysis (Tables 2, 3 and Fig. 7) shows that

Table 5
EIS graphical analysis method results at 50 °C.

Protein content (g/L)	C (μF/cm^2)	d (nm)	F_0 (mHz)	ρ_0 (Ohm.cm)	α
Starting OCP					
15	11	1	7.5	1.2×10^{14}	0.9
25	8	1.4	6	1.5×10^{14}	0.87
30	7.5	1.5	16	5×10^{13}	0.84
OCP after −0.9 V					
15	11	1	23	4×10^{13}	0.88
25	7	1.6	26	3.5×10^{13}	0.79
30	7	1.6	31	3×10^{13}	0.80

the oxide layer of the surfaces after polarization to −0.9 V exhibited lower resistance compared to that of the starting surface or the surface after a small cathodic potential (−0.7 V). The graphical analysis of EIS data (Tables 4, 5 and Fig. 11) shows that the resistivity of the oxide layer for the surfaces after −0.9 V polarization significantly decreased. Both analysis methods also revealed that the oxide layer exhibited less surface protection against corrosion with increasing temperature and increase in the protein concentration (i.e. a decrease in resistivity of the oxide layer was observed with increasing temperature and increasing protein content).

For the starting surface, the resistivity decreased with an increase in protein concentration for 37 °C and decreased between 25 and 30 g/L for 50 °C, Fig. 11. It is possible, but not confirmed experimentally in the current work, that chromium was preferentially dissolved with increasing protein concentration and temperature leading to a reduced resistivity of the oxide layer. Kocijan et al. [31] pointed out that protein can act as a complexing agent for dissolved ions of ASTM 304 and 316L stainless steel, facilitating further dissolution. They showed that some elements dissolve preferentially. Thus, the decrease in the resistivity of the oxide layer can be attributed to the depletion of the chromium in the outermost layer of the surface.

The thickness of the oxide layer was not affected by protein concentration or the cathodic polarization at 37 °C, Fig. 11. In contrast, at 50 °C, increasing the protein concentration resulted in a thickening of the oxide layer. However, the change in oxide film thickness was not associated with a change in resistivity, and therefore, it did not enhance the corrosion protective properties.

The same oxide layer thickness was observed before and after the polarization to −0.9 V, but the resistivity after polarization was significantly lower than before, see Fig. 11. In the current work, quantitative chemical composition analysis for the outermost surface after −0.9 V cathodic polarization at 30 g/L protein content solution and 50 °C, Fig. 16 and Table 6, show a small depletion of Cr just below the adsorbed proteinaceous layer. This possibly indicates that chromium preferentially dissolved at these cathodic potentials leading to the less resistive oxide layer. This suggests that the less resistive oxide is because of the depletion of chromium in the outermost surface due to the application of the cathodic potential.

The low resistance of the adsorbed protein layer at the starting OCP surfaces and the surfaces after −0.7 V cathodic polarization (Tables 2, 3 and Fig. 8) indicates a loose assembly of the protein molecules on the surface. The resistance of this layer increased with protein concentration only after −0.9 V cathodic polarization, indicating a more closely packed layer. A higher protein adsorption has also been observed for a CoCrMo alloy in protein-containing solution at the cathodic potential in comparison to passive potential by Muñoza and Mischler [15]. Li et al. [32] studied the depassivation-repassivation behaviour of CoCrMo alloys during tribocorrosion testing in protein-containing solutions. They pointed out that the adsorbed protein on the wear scar blocks the diffusion of the oxygen and consequently impedes the corrosion reactions.

It was shown through the QNM deformation map, Fig. 14, that the surface after −0.7 V cathodic polarization and 30 g/L protein concentration at 50 °C had very small areas with high deformation and low adhesion. The fraction of these areas increased for the surface after −0.9 V cathodic polarization and 15 g/L at 37 °C. For surface after −0.9 V cathodic polarization and 30 g/L at 50 °C these areas covered most of the surface. Vidal and Muñoz [18] have pointed out that the adsorption kinetics of bovine serum albumin on CoCrMo alloys is greatly affected by surface passivation in such a way that passive surface adsorbs less protein. This is in good agreement with the current results. The starting passive surfaces and the surfaces after −0.7 V adsorbed much less protein than ones after −0.9 V.

The question arises as to why the protein was adsorbed much more on the cathodically polarised surfaces, and why this adsorption increased with solution bulk protein concentration? The results of the current work are in an excellent agreement with the work of Muñoza and Mischler [15]. They have shown that applying cathodic potential in protein content solution led to adsorption of a thicker proteinaceous layer on the CoCrMo alloy compared to the passive potential. They related this to the electrochemical reduction of BSA. It has also been reported that the density of adsorbed protein depends on the bulk protein concentration in the solution [32]. This has been explained according to Ramsden [33] as follows: at low bulk concentration, the covering of the surface by absorbed protein is slow and therefore conformational and orientational changes in protein molecules might occur over adsorption. This obviously increases the protein's footprint on the surface during adsorption. In contrast, the covering of the surface at

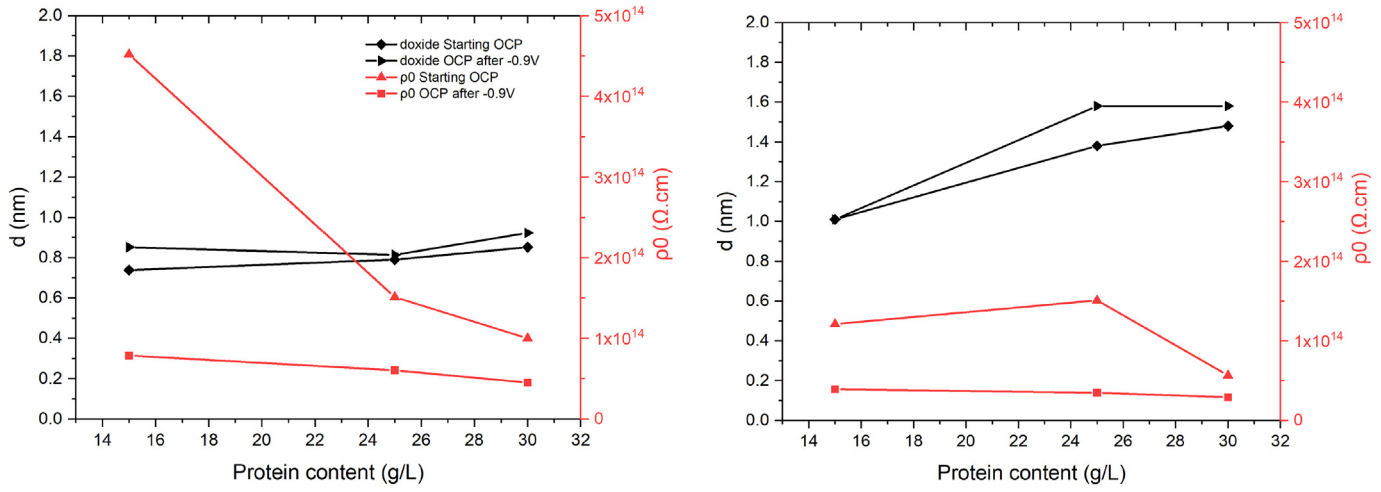

Fig. 11. Oxide film thickness and the resistivity at starting OCP and OCP after −0.9 V cathodic polarization at 37 °C (left hand graph) and 50 °C (right hand graph).

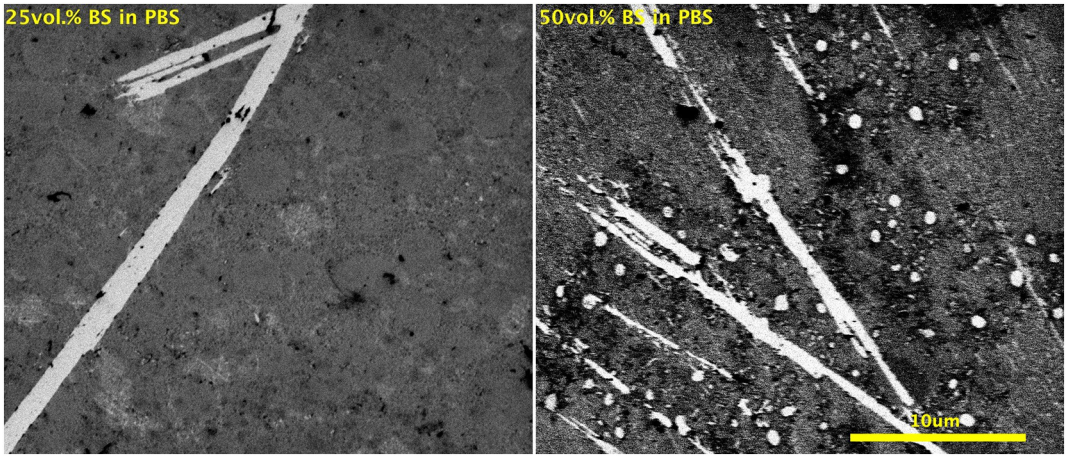

Fig. 12. SEM images for the surfaces after −0.9 V cathodic polarization for 15 g/L (on the left) and 30 g/L (on the right) solution protein content at 37°.

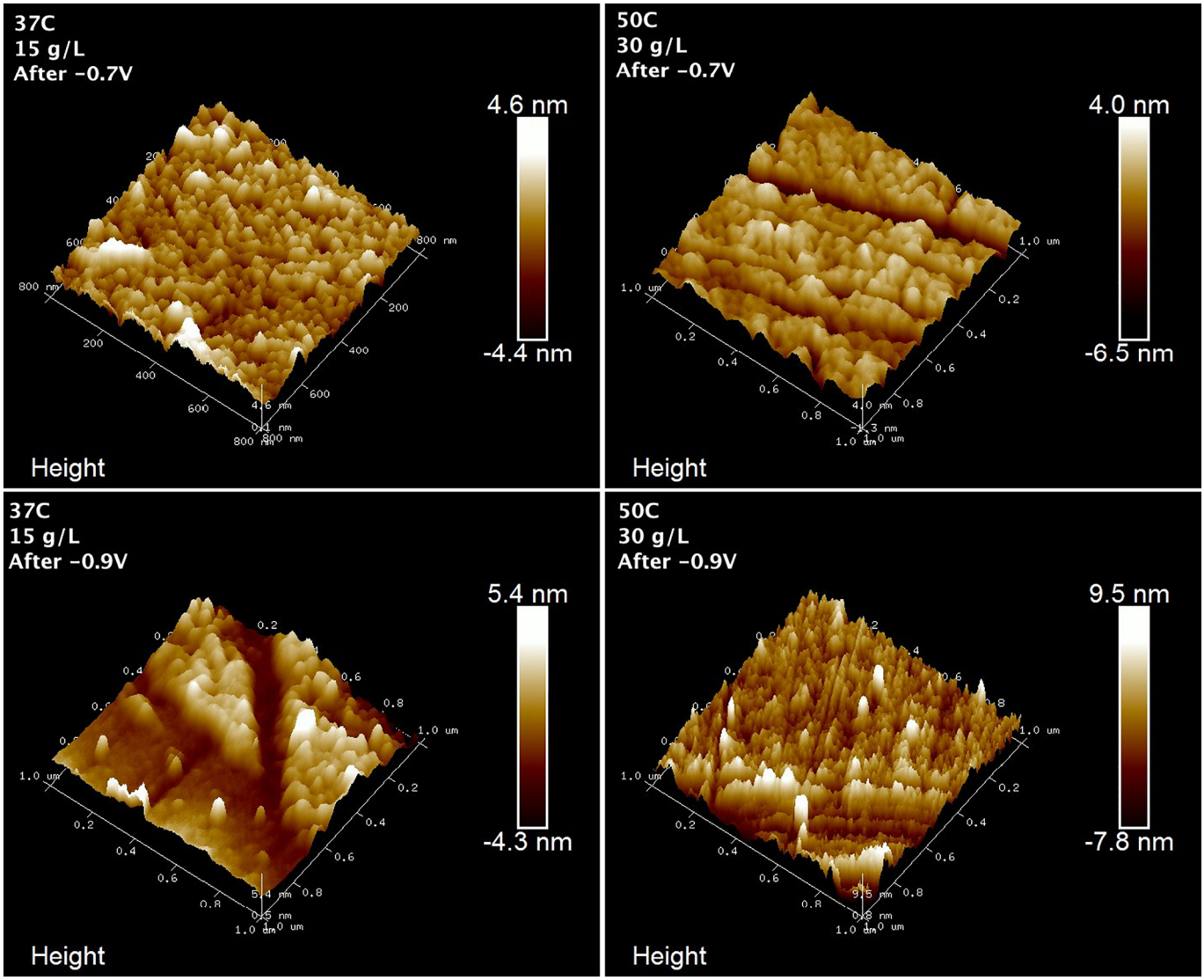

Fig. 13. Peak force tapping mode AFM imaging for the surfaces after different cathodic polarizations at selected protein content and temperature for sake of comparison.

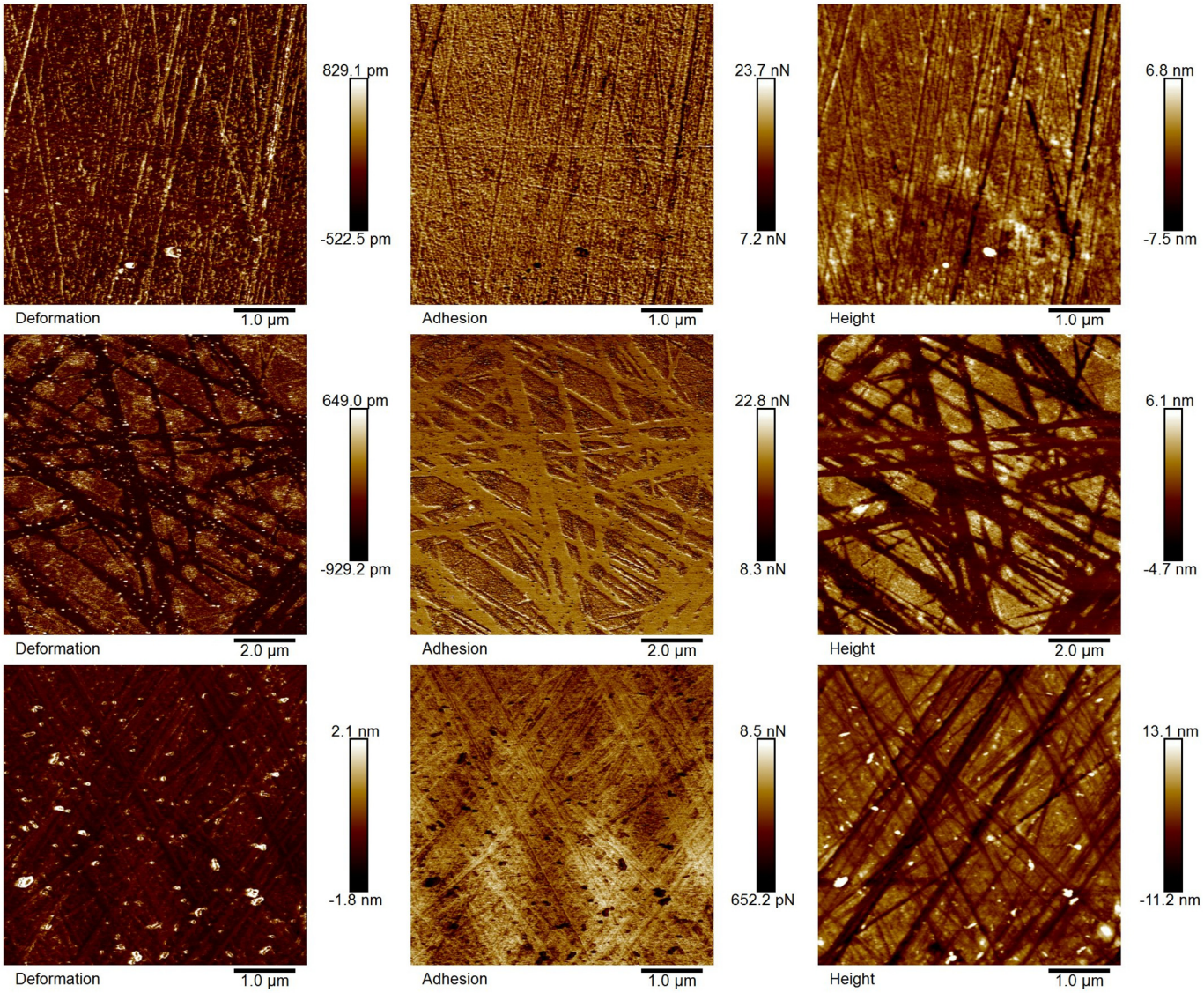

Fig. 14. Peak force QNM with height maps for the surfaces after different cathodic polarizations. The upper row is for the sample after −0.7 V 15 g/L protein at 50 °C. The middle row is for the sample after −0.9 V 15 g/L protein, at 37 °C and the lower row is for 30 g/L protein after −0.9 V at 50 °C.

high bulk protein concentration solution occurs quickly, which effectively hinders the structural changes of the protein leading to the formation of a highly saturated adsorbed layer. Additionally, the assembly of the protein on the surface is greatly influenced by pH and bulk concentration expressed by ionic strength [34]. A loosely assembled layer is achieved at low ionic strength, whereas high ionic strength leads to the formation of a densely packed layer by shielding some of the repulsive forces among molecules [35]. It should be noted here that the protein molecules in this work were negatively charged, as the isostatic point for bovine serum albumin is 4.5 [10] and the solution pH was buffered to 7.4. Thus, the effect of pH on the assembly of protein on the surface in the current work was limited.

Quantitative nanomechanical adhesion maps (Fig. 14) revealed that the adhesion of the thicker adsorbed layer was much less than that for the thinner one. This result suggests that the adsorbed layer affects the friction in a beneficial manner and may also affect the wear behaviour of this material. To this end, the tribocorrosion behaviour for these surfaces is not clear and it needs further investigation.

5. Conclusions

1. Increasing protein concentration and temperature caused a significant drop in oxide film resistance and metal surface/oxide layer resistivity. However, there was no reduction of the oxide film thickness.
2. Polarising the surface to a small cathodic potential of −0.7 V did not greatly affect the resistance of the surface oxide film when measured after this potential was removed.
3. Polarising the surface to a higher cathodic potential of −0.9 V led to a significant drop in the resistance and resistivity of the oxide film for the surfaces when measured after this potential was removed. The thickness of the oxide layer after this cathodic polarization did not change appreciably. The drop in resistivity corresponded to a small, but significant, change in surface chemical composition due to this cathodic polarization.
4. Surfaces with thicker adsorbed layer exhibited fewer adhesion forces. This suggests that the adsorbed layer might work as a solid lubricant and be useful in tribocorrosion applications.

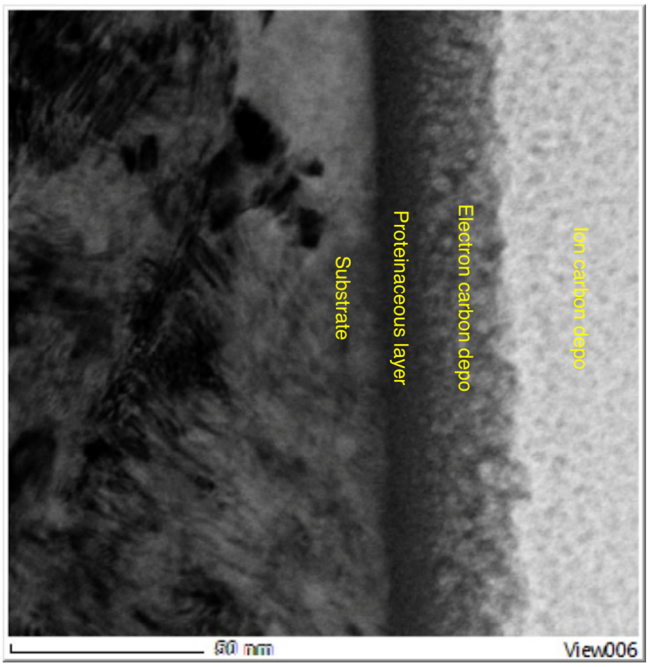

Fig. 15. Bright field STEM image for the surface after −0.9 V cathodic polarization at 30 g/L protein content solution and 50 °C.

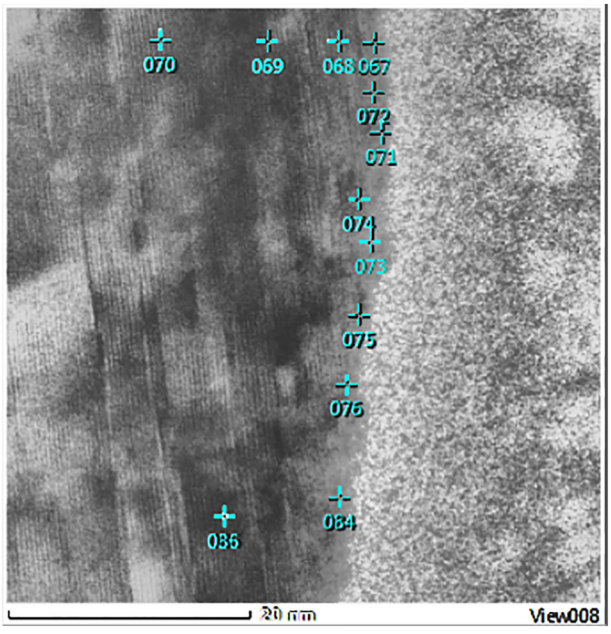

Fig. 16. Bright field STEM images shows EDS quantitative chemical composition spot analysis points for the surface after −0.9 V cathodic polarization at 30 g/L protein content solution and 50 °C. See Table 6 for the compositions corresponding to the numbered locations.

Declaration of competing interest

We have no conflicts of interest to disclose.

Acknowledgement

We wish to acknowledge the Henry Royce Institute for Advanced Materials (EPSRC Grant Number EP/R00661X/1) for the financial support and equipment access at Royce@Sheffield.

Table 6
EDS quantitative chemical composition for the surface after −0.9 V cathodic polarization at 30 g/L protein content solution and 50 °C for many closest points to the surface and others on the bulk points which are.

Points		Cr K	Co K	Mo L
67 (surface)	Mass%	23.48	68.48	8.05
	Atom%	26.6	68.46	4.94
71 (surface)	Mass%	23.78	69.77	6.45
	Atom%	26.77	69.3	3.94
72 (surface)	Mass%	23.08	69.11	7.81
	Atom%	26.14	69.06	4.8
73 (surface)	Mass%	22.35	69.61	8.03
	Atom%	25.36	69.69	4.94
74 (surface)	Mass%	23.66	66.89	9.45
	Atom%	26.95	67.22	5.83
75 (surface)	Mass%	24.41	66.51	9.08
	Atom%	27.74	66.67	5.59
78 (surface)	Mass%	23.34	66.37	10.29
	Atom%	26.69	66.94	6.37
84 (surface)	Mass%	23.81	64.9	11.29
	Atom%	27.31	65.67	7.02
68 (Close to the surface)	Mass%	24.83	65.46	9.7
	Atom%	28.27	65.75	5.99
69 (Substrate)	Mass%	25.64	67.41	6.95
	Atom%	28.85	66.92	4.24
70 (Substrate)	Mass%	25.34	65.37	9.3
	Atom%	28.78	65.5	5.72
86 (Substrate)	Mass%	27.17	66.37	6.46
	Atom%	30.45	65.62	3.93

References

[1] H. McKellop, et al., In vivo wear of three types of metal on metal hip prostheses during two decades of use, Clin. Orthop. Relat. Res. (Aug. 1996) S128–S140 no. 329 Suppl.
[2] S.R. Brown, I. Adam, Intestinal obstruction, Surg 20 (7) (Jul. 2002) 157–164.
[3] J. Daniel, C. Pradhan, H. Ziaee, P.B. Pynsent, D.J.W. McMinn, Results of Birmingham hip resurfacing at 12 to 15 years, Bone Joint J 96-B (10) (Oct. 2014) 1298–1306.
[4] A.J. Smith, P. Dieppe, P.W. Howard, A.W. Blom, Failure rates of metal-on-metal hip resurfacings: analysis of data from the National Joint Registry for England and Wales, Lancet 380 (9855) (Nov. 2012) 1759–1766.
[5] R. Sharma, et al., Meta-analyses in joint arthroplasty: a review of quantity, quality, and impact, J. Bone Jt. Surg. - Ser. A 93 (24) (Dec. 2011) 2304–2309.
[6] L. Ma, Wear Behaviour of Biolox Delta Ceramic Composite for Joint Replacements, no. January The University of Sheffield, 2010.
[7] C. Lentner, Geigy scientific tables, Geigy Sci. Tables, 2014, pp. 1–41.
[8] G. Bergmann, F. Graichen, J. Dymke, A. Rohlmann, G.N. Duda, P. Damm, High-tech hip implant for wireless temperature measurements in vivo, PLoS One 7 (8) (2012) e43489Aug.
[9] N.P. Cosman, K. Fatih, S.G. Roscoe, Electrochemical impedance spectroscopy study of the adsorption behaviour of α-lactalbumin and β-casein at stainless steel, J. Electroanal. Chem. 574 (2) (2005) 261–271 Jan.
[10] S. Omanovic, S.G. Roscoe, Electrochemical studies of the adsorption behavior of bovine serum albumin on stainless steel, Langmuir 15 (23) (1999) 8315–8321 Nov.
[11] C. Valero Vidal, A. Igual Muñoz, Influence of protein adsorption on corrosion of biomedical alloys, Bio-Tribocorrosion in Biomaterials and Medical Implants, Elsevier, 2013, pp. 187–219.
[12] M.M. Ouberai, K. Xu, M.E. Welland, Effect of the interplay between protein and surface on the properties of adsorbed protein layers, Biomaterials 35 (24) (2014) 6157–6163. Aug.
[13] B. Clarke, P. Kingshott, X. Hou, Y. Rochev, A. Gorelov, W. Carroll, Effect of nitinol wire surface properties on albumin adsorption, Acta Biomater. 3 (1) (2007) 103–111 Jan.
[14] M. Rabe, D. Verdes, S. Seeger, Understanding protein adsorption phenomena at solid surfaces, Adv. Colloid Interf. Sci. 162 (1–2) (2011) 87–106 Feb.
[15] A.I. Muñoz, S. Mischler, Electrochemical quartz crystal microbalance and X-ray photoelectron spectroscopy study of cathodic reactions in bovine serum albumin containing solutions on a physical vapour deposition-CoCrMo biomedical alloy, Electrochim. Acta 180 (2015) 96–103 Oct.
[16] D.R. Jackson, S. Omanovic, S.G. Roscoe, Electrochemical studies of the adsorption behavior of serum proteins on titanium, Langmuir 16 (12) (2000) 5449–5457 Jun.
[17] C. Valero Vidal, A. Olmo Juan, A. Igual Muñoz, Adsorption of bovine serum albumin on CoCrMo surface: effect of temperature and protein concentration, Colloids Surfaces B Biointerfaces 80 (1) (Oct. 2010) 1–11.
[18] C. Valero Vidal, A. Igual Muñoz, Study of the adsorption process of bovine serum albumin on passivated surfaces of CoCrMo biomedical alloy, Electrochim. Acta 55 (28) (2010) 8445–8452 Dec.
[19] A.I. Muñoz, S. Mischler, Interactive effects of albumin and phosphate ions on the

corrosion of CoCrMo implant alloy, J. Electrochem. Soc. 154 (10) (Oct. 2007) C562.
[20] P. Zoltowski, On the electrical capacitance of interfaces exhibiting constant phase element behaviour, J. Electroanal. Chem. 443 (1) (1998) 149–154 Feb.
[21] M.E. Orazem, B. Tribollet, Electrochemical Impedance Spectroscopy, John Wiley & Sons, Inc., Hoboken, NJ, USA, 2008.
[22] M. Itagaki, S. Suzuki, I. SHITANDA, W. Kunihiro, K. WATANABE, Electrochemical impedance and complex capacitance to interpret electrochemical capacitor, Electrochemistry 75 (8) (Aug. 2007) 649–655.
[23] J. Baux, et al., Impedance analysis of film-forming amines for the corrosion protection of a carbon steel, Electrochim. Acta 283 (2018) 699–707 Sep.
[24] M. Benoit, et al., Comparison of different methods for measuring the passive film thickness on metals, Electrochim. Acta 201 (2016) 340–347 May.
[25] T. Barrès, B. Tribollet, O. Stephan, H. Montigaud, M. Boinet, Y. Cohin, Characterization of the porosity of silicon nitride thin layers by electrochemical impedance spectroscopy, Electrochim. Acta 227 (2017) 1–6 Feb.
[26] S. Chakri, et al., Improved EIS analysis of the electrochemical behaviour of carbon steel in alkaline solution, Electrochim. Acta 246 (2017) 924–930. Aug.
[27] P.H. Fang, W.S. Brower, Dielectric constant of Cr2O3 crystals, Phys. Rev. 129 (4) (1963) 1561 Feb.
[28] A.W.E.W.E. Hodgson, S. Kurz, S. Virtanen, V. Fervel, C.-O.A.O. a Olsson, S. Mischler, Passive and transpassive behaviour of CoCrMo in simulated biological solutions, Electrochim. Acta 49 (13) (May 2004) 2167–2178.
[29] B. Hirschorn, M.E. Orazem, B. Tribollet, V. Vivier, I. Frateur, M. Musiani, Constant-phase-element behavior caused by resistivity distributions in films: I. Theory, J. Electrochem. Soc. 157 (12) (Dec. 2010) C452–C457.
[30] Asm, ASM Handbook Volume 2: Properties and Selection: Nonferrous Alloys and Special-Purpose Materials, no. v. 3, (1986).
[31] A. Kocijan, I. Milošev, B. Pihlar, The influence of complexing agent and proteins on the corrosion of stainless steels and their metal components, J. Mater. Sci. Mater. Med 14 (1) (2003) 69–77.
[32] X. Li, Y. Yan, H. Zhang, Y. Su, L. Q.- INTERNATIONAL, and undefined 2017, "Depassivation–Repassivation Behavior of a CoCrMo Alloy Under Tribological Contact in Simulated Body Fluids," *electrochemsci.org*.
[33] J.J. Ramsden, Puzzles and paradoxes in protein adsorption, Chem. Soc. Rev. 24 (1) (1995) 73 Jan.
[34] E. Brynda, V. Hlady, J.D. Andrade, Protein packing in adsorbed layers studied by excitation energy transfer, J. Colloid Interface Sci. 139 (2) (1990) 374–380 Oct.
[35] K.L. Jones, C.R. O'Melia, Protein and humic acid adsorption onto hydrophilic membrane surfaces: effects of pH and ionic strength, J. Memb. Sci 165 (1) (2000) 31–46 Jan.